PHYSICAL REVIEW D **76,** 123004 (2007)

Cosmological observables in a Swiss-cheese universe

Valerio Marra[*]

Dipartimento di Fisica "G. Galilei" Università di Padova, INFN Sezione di Padova, via Marzolo 8, Padova I-35131, Italy
Department of Astronomy and Astrophysics, The University of Chicago, Chicago, Illinois 60637-1433, USA

Edward W. Kolb[†]

Department of Astronomy and Astrophysics, Enrico Fermi Institute, Kavli Institute for Cosmological Physics, The University of Chicago, Chicago, Illinois 60637-1433, USA

Sabino Matarrese[‡]

Dipartimento di Fisica "G. Galilei" Università di Padova, INFN Sezione di Padova, via Marzolo 8, Padova I-35131, Italy

Antonio Riotto[§]

Département de Physique Théorique, Université de Gèneve, 24 Quai Ansermet, Gèneve, Switzerland, and INFN Sezione di Padova, via Marzolo 8, Padova I-35131, Italy

(Received 3 September 2007; published 5 December 2007)

Photon geodesics are calculated in a Swiss-cheese model, where the cheese is made of the usual Friedmann-Robertson-Walker (FRW) solution and the holes are constructed from a Lemaître-Tolman-Bondi solution of Einstein's equations. The observables on which we focus are the changes in the redshift, in the angular-diameter-distance relation, in the luminosity-distance-redshift relation, and in the corresponding distance modulus. We find that redshift effects are suppressed when the hole is small because of a compensation effect acting on the scale of half a hole resulting from the special case of spherical symmetry. However, we find interesting effects in the calculation of the angular distance: strong evolution of the inhomogeneities (as in the approach to caustic formation) causes the photon path to deviate from that of the FRW case. Therefore, the inhomogeneities are able to partly mimic the effects of a dark-energy component. Our results also suggest that the nonlinear effects of caustic formation in cold dark matter models may lead to interesting effects on photon trajectories.

DOI: 10.1103/PhysRevD.76.123004 PACS numbers: 95.36.+x, 98.80.−k

I. INTRODUCTION

In this paper we explore a toy cosmological model in order to attempt to understand the role of large-scale nonlinear cosmic inhomogeneities in the interpretation of observable data. The model is based on a Swiss-cheese model, where the cheese consists of the usual Friedmann-Robertson-Walker (FRW) solution and the holes are constructed out of a Lemaître-Tolman-Bondi (LTB) solution. The advantage of this model is that it is a solvable model with strong nonlinearities, in particular, the formation of caustics as expected in the cold dark matter (CDM) models.

Most, if not all, observations are consistent with the cosmic concordance model according to which, today, one-fourth of the mass-energy of the universe is clustered and dominated by cold dark matter. The remaining three-quarters is uniform and dominated by a fluid with a negative pressure (dark energy, or Λ).

While the standard ΛCDM model seems capable of accounting for the observations, it does have the feature that approximately 95% of the mass-energy of the present universe is unknown. We are either presented with the opportunity of discovering the nature of dark matter and dark energy, or nature might be different than described by the ΛCDM model. Regardless, until such time as dark matter and dark energy are completely understood, it is useful to look for alternative cosmological models that fit the data.

One nonstandard possibility is that there are large effects on the *observed* expansion rate due to the backreaction of inhomogeneities in the universe. The basic idea is that all evidence for dark energy comes from observational determination of the expansion history of the universe. Anything that affects the observed expansion history of the universe alters the determination of the parameters of dark energy; in the extreme it may remove the need for dark energy.

This paper focuses on the effects of large-scale nonlinear inhomogeneities on observables such as the luminosity-distance-redshift relation. The ultimate goal is to find a realistic dust model that can explain observations (like the luminosity-distance-redshift relation) without the need of dark energy. The ultimate desire will be to have an exactly solvable realistic inhomogeneous model. Our model is but a first small step in this pragmatic and necessary direction.

If this first step is successful, we would show that inhomogeneities must be factored into the final solution.

[*]valerio.marra@pd.infn.it
[†]rocky.kolb@uchicago.edu
[‡]sabino.matarrese@pd.infn.it
[§]antonio.riotto@pd.infn.it

Even if we live in a ΛCDM universe, inhomogeneities ''renormalize'' the theory adding an effective extra source to the dark energy. We have to be very careful in what we mean. The inhomogeneities renormalize the dust Einstein-de Sitter universe only from the observational point of view, that is luminosity and redshift of photons. Average dynamics is beyond this and we will not be concerned with this issue in this paper: if we find an effective cosmological constant, this will not mean that the universe is accelerating, but only that its luminosity-distance-redshift relation will fit the observational data.

Here we are not primarily interested in the backreaction effect that comes from the averaging procedure in general relativity (see e.g. [1]). Since we have an exact solution, we can directly calculate observables. Indeed, in this paper we are mainly interested in the effect of inhomogeneities on the dynamics of photons.

We can reformulate our present approach as follows: inhomogeneities renormalize the geodesics of photons. In the extreme case in which such a renormalization leads to a negative effective deceleration parameter in the luminosity-distance-redshift relation, it might make us think that a dark-energy component exists.

The paper is organized as follows: In Sec. II we will specify the parameters of our Swiss-cheese model. In Sec. III we study its dynamics. Then in Sec. IV we will discuss the geodesic equations for light propagation. We will apply them to see what an observer in the cheese (Sec. V) or in the hole (Sec. VI) would observe. The observables on which we will focus are the change in redshift Δz, angular-diameter-distance $\Delta d_A(z)$, luminosity-distance-redshift relation $\Delta d_L(z)$, and the distance modulus $\Delta m(z)$.

Conclusions are given in Sec. VII. In two appendices we discuss the role of arbitrary functions in LTB models (Appendix A) and some technical issues in the solution of photon geodesics in our Swiss-cheese model (Appendix B).

II. THE MODEL

We study a Swiss-cheese model where the cheese consists of the usual Friedmann-Robertson-Walker solution and the spherically symmetric holes are constructed from a Lemaître-Tolman-Bondi solution. The particular FRW solution we will choose is a matter-dominated, spatially flat solution, i.e., the Einstein-de Sitter (EdS) model.

In this section we will describe the FRW and LTB model parameters we have chosen. But first, in Table I we list the units we will use for mass density, time, the radial coordinate, the expansion rate, and two quantities, $Y(r, t)$ and $W(r)$, that will appear in the metric.

The time t appearing in Table I is not the usual time in FRW models. Rather, $t = T - T_0$, where T *is* the usual cosmological time and $T_0 = 2H_0^{-1}/3$ is the present age of the universe. Thus, $t = 0$ is the present time and $t = t_{BB} = -T_0$ is the time of the big bang. Finally, the initial time of the LTB evolution is defined as $\bar{t}$.

Both the FRW and the LTB metrics can be written in the form

$$ds^2 = -dt^2 + \frac{Y'^2(r, t)}{W^2(r)}dr^2 + Y^2(r, t)d\Omega^2, \qquad (1)$$

where here and throughout, the ''prime'' superscript denotes d/dr and the ''dot'' superscript will denote d/dt. It is clear that the Robertson-Walker metric is recovered with the substitution $Y(r, t) = a(t)r$ and $W^2(r) = 1 - kr^2$.

The above metric is expressed in the synchronous and comoving gauge.

A. The cheese

We choose for the cheese model a spatially flat, matter-dominated universe (the EdS model). So in the cheese there is no r dependence to ρ or H. Furthermore, $Y(r, t)$ factors into a function of t multiplying r ($Y(r, t) = a(t)r$), and in the EdS model $W(r) = 1$. In this model $\Omega_M = 1$, so in the cheese, the value of ρ today, denoted as ρ_0, is unity in the units of Table I. In order to connect with the LTB solution, we can express the line element in the form

$$ds^2 = -dt^2 + Y'^2(r, t)dr^2 + Y^2(r, t)d\Omega^2. \qquad (2)$$

In the cheese, the Friedmann equation and its solution are (recall $t = 0$ corresponds to the present time):

$$H^2(t) = \tfrac{4}{9}\rho(t) = \tfrac{4}{9}(t + 1)^{-2}, \qquad (3)$$

TABLE I. Units for various quantities. We use geometrical units, $c = G = 1$. Here, the present critical density is $\rho_{C0} = 3H_{0,\mathrm{Obs}}^2/8\pi$, with $H_{0,\mathrm{Obs}} = 70\ \mathrm{kms}^{-1}\,\mathrm{Mpc}^{-1}$.

Quantity	Notation	Unit	Value
Mass density	$\rho(r, t)$, $\bar{\rho}(r, t)$	ρ_{C0}	$9.2 \times 10^{-30}\ \mathrm{g\,cm}^{-3}$
Time	t, T, $\bar{t}$, t_{BB}, T_0	$(6\pi\rho_{C0})^{-1/2}$	9.3 Gyr
Comoving radial coordinate	r	$(6\pi\rho_{C0})^{-1/2}$	2857 Mpc
Metric quantity	$Y(r, t)$	$(6\pi\rho_{C0})^{-1/2}$	2857 Mpc
Expansion rate	$H(r, t)$	$(6\pi\rho_{C0})^{1/2}$	$\frac{3}{2}H_{0,\mathrm{Obs}}$
Spatial curvature term	$W(r)$	1	—

$$Y(r,t) = ra(t) = r\frac{(t+1)^{2/3}}{(\bar{t}+1)^{2/3}}, \tag{4}$$

where the scale factor is normalized so that at the beginning of the LTB evolution it is $a(\bar{t}) = 1$.

For the EdS model, $T_0 = 1$. We also note that the comoving distance traveled by a photon since the big bang is $r_{BB} = 3/a_0$.

B. The holes

The holes are chosen to have an LTB metric [2–4]. The model is based on the assumptions that the system is spherically symmetric with purely radial motion and the motion is geodesic without shell crossing (otherwise we could not neglect the pressure).

It is useful to define a "Euclidean" mass $M(r)$ and an "average" mass density $\bar{\rho}(r,t)$, defined as

$$M(r) = 4\pi\int_0^r \rho(r,t)Y^2Y'dr = \frac{4\pi}{3}Y^3(r,t)\bar{\rho}(r,t). \tag{5}$$

In spherically symmetric models, in general there are two expansion rates: an angular expansion rate, $H_\perp \equiv \dot{Y}(r,t)/Y(r,t)$, and a radial expansion rate, $H_r \equiv \dot{Y}'(r,t)/Y'(r,t)$. (Of course in the FRW model $H_r = H_\perp$.) The angular expansion rate is given by

$$H_\perp^2(r,t) = \frac{4}{9}\bar{\rho}(r,t) + \frac{W^2(r)-1}{Y^2(r,t)}. \tag{6}$$

Unless specified otherwise, we will identify $H_\perp = H$.

To specify the model we have to specify initial conditions, i.e., the position $Y(r,\bar{t})$, the velocity $\dot{Y}(r,\bar{t})$, and the density $\rho(\bar{t})$ of each shell r at time $\bar{t}$. In the absence of shell crossing it is possible to give the initial conditions at different times for different shells r: let us call this time $\bar{t}(r)$. The initial conditions fix the arbitrary curvature function $W(r)$:

$$W^2(r) - 1 \equiv 2E(r) = \left(\dot{Y}^2 - \frac{1}{3\pi}\frac{M}{Y}\right)\Big|_{r,\bar{t}}, \tag{7}$$

where we can choose $Y(r,\bar{t}) = r$ so that $M(r) = 4\pi\int_0^r \rho(\bar{r},\bar{t})\bar{r}^2 d\bar{r}$.

In a general LTB model there are therefore three arbitrary functions: $\rho(r,\bar{t})$, $W(r)$, and $\bar{t}(r)$. Their values for the particular LTB model we study are specified in the following subsection.

In Appendix A we provide a discussion about the number of independent arbitrary functions in a LTB model.

Our LTB model

First of all, for simplicity we choose $\bar{t}(r) = \bar{t}$; i.e., we specify the initial conditions for each shell at the same moment of time.

We now choose $\rho(r,\bar{t})$ and $W(r)$ in order to match the flat FRW model at the boundary of the hole: i.e., at the boundary of the hole $\bar{\rho}$ has to match the FRW density and $W(r)$ has to go to unity. A physical picture is that, given a FRW sphere, all the matter in the inner region is pushed to the border of the sphere while the quantity of matter inside the sphere does not change. With the density chosen in this way, an observer outside the hole will not feel the presence of the hole as far as *local* physics is concerned (this does not apply to global quantities, such the luminosity-distance-redshift relation, for example). So the cheese is evolving as a FRW universe while the holes evolve differently. In this way we can imagine putting in the cheese as many holes as we want, even with different sizes and density profiles, and still have an exact solution of the Einstein equations (as long as there is no superposition among the holes and the correct matching is achieved). The limiting picture of this procedure is the Apollonian Gasket of Fig. 1, where all the possible holes are placed, and therefore the model has the strange property that it is FRW nowhere, but it behaves as a FRW model on the average. This idea was first proposed by Einstein and Straus [5].

To be specific, we choose $\rho(r,\bar{t})$ to be

$$\begin{aligned} &\rho(r,\bar{t}) = A\exp[-(r-r_M)^2/2\sigma^2] + \epsilon \quad (r < r_h),\\ &\rho(r,\bar{t}) = \rho_{\mathrm{FRW}}(\bar{t}) \quad (r > r_h), \end{aligned} \tag{8}$$

where $\epsilon = 0.0025$, $r_h = 0.42$, $\sigma = r_h/10$, $r_M = 0.037$, $A = 50.59$, and $\rho_{\mathrm{FRW}}(\bar{t}) = 25$. In Fig. 2 we plot this chosen Gaussian density profile. The hole ends at $r_h = 0.042$ which is [6] 350 Mpc and roughly 25 times smaller than r_{BB}. Note that this is not a very big bubble. But it is an almost empty region: in the interior the matter density is roughly 10^4 times smaller than in the cheese. Our model consists of a sequence of up to five holes and the observer is looking through them. The idea, however, is that the

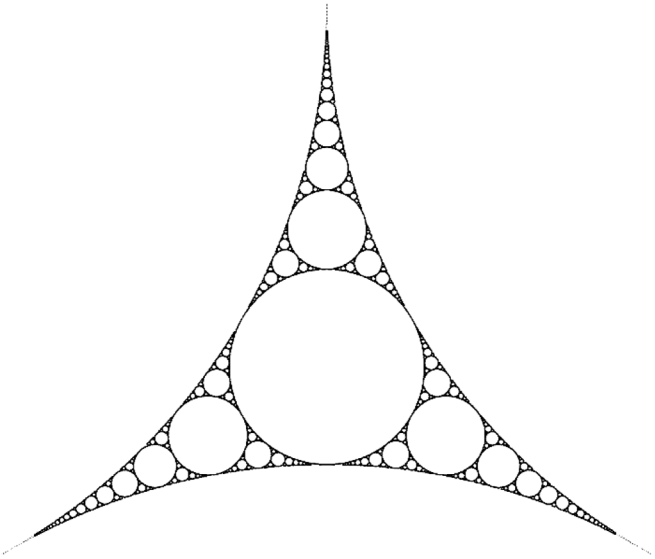

FIG. 1. The Apollonian gasket.

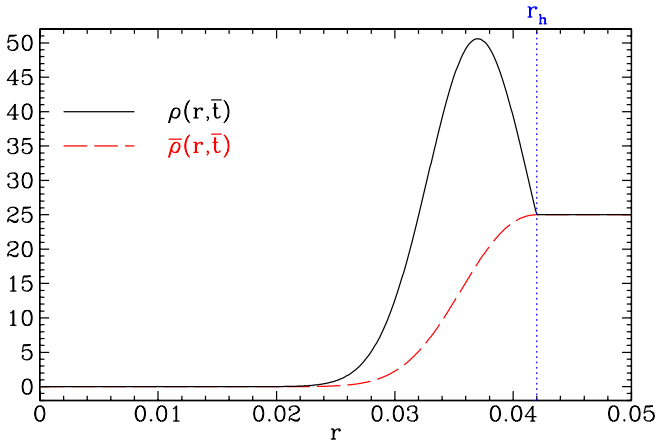

FIG. 2 (color online). The densities $\rho(r, \bar{t})$ (solid curve) and $\bar{\rho}(r, \bar{t})$ (dashed curve). Here, $\bar{t} = -0.8$ (recall $t_{BB} = -1$). The hole ends at $r_h = 0.042$. The matching to the FRW solution is achieved as one can see from the plot of $\bar{\rho}(r, \bar{t})$.

universe is completely filled with these holes, which form a sort of lattice as shown in Fig. 3. In this way an observer at rest with respect to a comoving cheese-FRW observer will see an isotropic CMB along the two directions of sight shown in Fig. 3.

It is useful to consider the velocity of a shell relative to the FRW background. We define

$$\Delta v_{sh}(r, t) = \dot{a}_{\mathrm{LTB}}(r, t) - \dot{a}_{\mathrm{FRW}}(t), \tag{9}$$

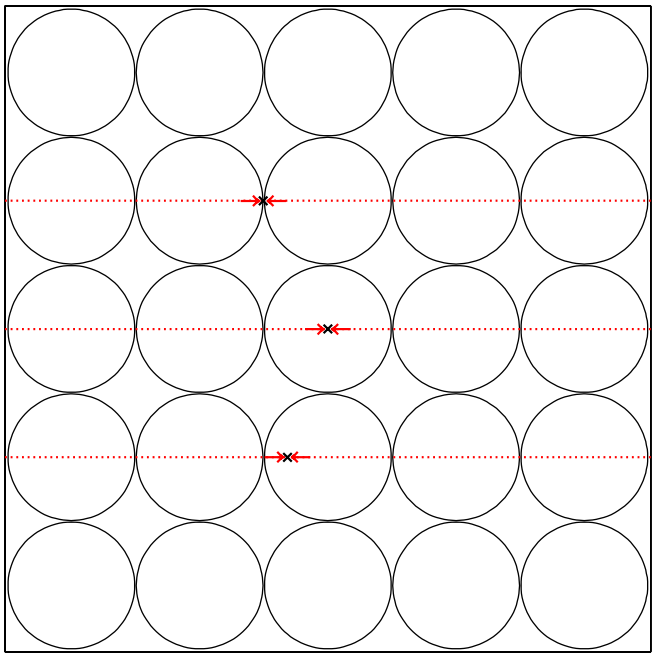

FIG. 3 (color online). Sketch of our Swiss-cheese model. An observer at rest with respect to a comoving cheese-FRW observer will see an isotropic CMB along the two directions of sight marked with dotted red lines. Three possible positions for an observer are shown.

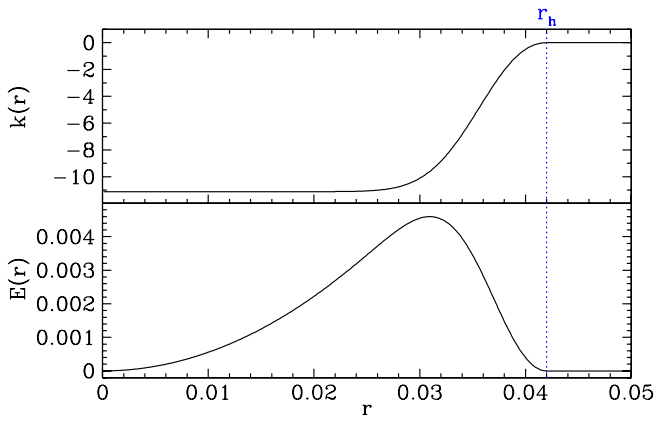

FIG. 4 (color online). Curvature $E(r)$ and $k(r)$ necessary for the initial conditions of no peculiar velocities.

where $a_{\mathrm{LTB}}(r, t) = Y(r, t)/r$. To have a realistic evolution, we demand that there are no initial peculiar velocities at time $\bar{t}$, that is, to have an initial expansion H independent of r: $\Delta v_{sh}(r, \bar{t}) = 0$. From Eq. (7) this implies

$$E(r) = \frac{1}{2} H_{\mathrm{FRW}}^2(\bar{t}) r^2 - \frac{1}{6\pi} \frac{M(r)}{r}. \tag{10}$$

The graph of $E(r)$ chosen in this way is shown in Fig. 4. As seen from the figure, the curvature $E(r)$ is small compared with unity. Indeed, in many formulae $W = (1 + 2E)^{1/2} \simeq 1 + E$ appears, therefore one should compare E with 1. In spite of its smallness, the curvature will play a crucial role to allow a realistic evolution of structures, as we will see in the next section.

Also in Fig. 4 we graph $k(r) = -2E(r)/r^2$, which is the generalization of the factor k in the usual FRW models. (It is not normalized to unity.) As one can see, $k(r)$ is very nearly constant in the empty region inside the hole. This is another way to see the reason for our choice of the curvature function: we want to have in the center an empty bubble dominated by negative curvature.

It is important to note that the dynamics of the hole is scale independent: small holes will evolve in the same way as big holes. To show this, we just have to express Eq. (6) with respect to a generic variable $\tilde{r} = r/g$ where g fixes the scale. If we change g, i.e., scale the density profile, we will find the same scaled shape for $k(r)$ and the same time evolution. This property is again due to spherical symmetry which frees the inner shells from the influence of the outer ones: We can think of a shell as an infinitesimal FRW solution and its behavior is scale independent because it is a homogeneous and isotropic solution.

III. THE DYNAMICS

Now we explore the dynamics of this Swiss-cheese model. As we have said, the cheese evolves as in the standard FRW model. Of course, inside the holes the

evolution is different. This will become clear from the plots given below.

We will discuss two illustrative cases: a flat case where $E(r) = 0$, and a curved case where $E(r)$ is given by Eq. (10). We are really interested only in the second case because the first will turn out to be unrealistic. But the flat case is useful to understand the dynamics.

A. The flat case

In Fig. 5 we show the evolution of $Y(r, t)$ for the flat case, $E(r) = 0$. In the figure $Y(r, t)$ is plotted for 3 times: $t = \bar{t} = -0.8$ (recall $t_{BB} = -1$), $t = -0.4$, and $t = 0$ (corresponding to today).

From Fig. 5 it is clear that outside the hole, i.e., for $r \geq r_h$, $Y(r, t)$ evolves as a FRW solution, $Y(r, t) \propto r$. However, deep inside the hole where it is almost empty, there is no time evolution to $Y(r, t)$: it is Minkowski space. Indeed, thanks to spherical symmetry, the outer shells do not influence the interior. If we place additional matter inside the empty space, it will start expanding as a FRW universe, but at a lower rate because of the lower density. It is interesting to point out that a photon passing the empty region will undergo no redshift; again, it is just Minkowski space.

This counterintuitive behavior (empty regions expanding slowly) is due to the fact that the spatial curvature vanishes. This corresponds to an unrealistic choice of initial peculiar velocities. To see this we plot the peculiar velocity that an observer following a shell r has with respect to a FRW observer passing through that same spatial point. The result is also shown in Fig. 5 where it is seen that matter is escaping from the high-density regions. This causes the evolution to be reversed as one can see in Fig. 5 from the density profile at different times: structures are not forming, but spreading out.

Remember that r is only a label for the shell whose Euclidean position at time t is $Y(r, t)$. In the plots of the energy density we have normalized $Y(r, t)$ using $r_{\mathrm{FRW}} = Y(r, t)/a(t)$.

B. The curved case

Now we move to a more interesting and relevant case. We are going to use the $E(r)$ given by Eq. (10); the other parameters will stay the same. Comparison with the flat

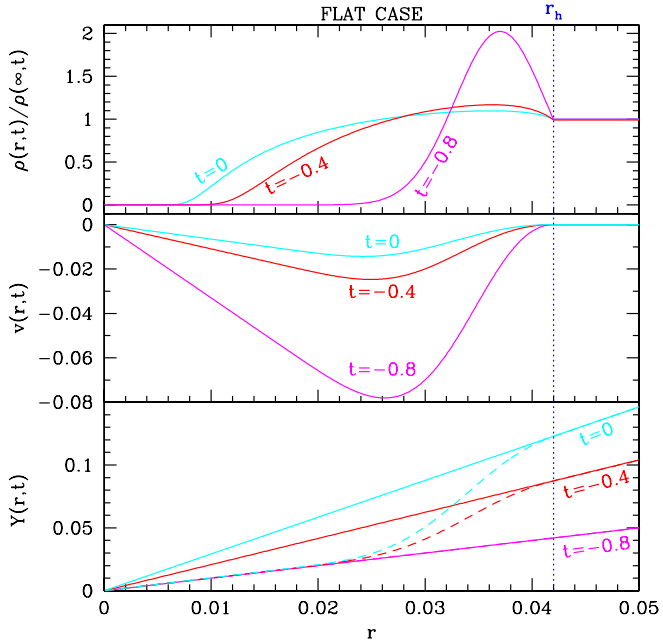

FIG. 5 (color online). Behavior of $Y(r, t)$ with respect to r, the peculiar velocities $v(r, t)$ with respect to r, and the density profiles $\rho(r, t)$ with respect to $r_{\mathrm{FRW}} = Y(r, t)/a(t)$, for the flat case at times $t = \bar{t} = -0.8$, $t = -0.4$, and $t = t_0 = 0$. The straight lines for $Y(r, t)$ are the FRW solutions while the dashed lines are the LTB solutions. For the peculiar velocities, matter is escaping from high-density regions. The center has no peculiar velocity because of spherical symmetry, and the maximum of negative peculiar velocity is before the peak in density. Finally, the values of $\rho(\infty, t)$ are 1, 2.8, and 25, for $t = 0$, -0.4, -0.8, respectively.

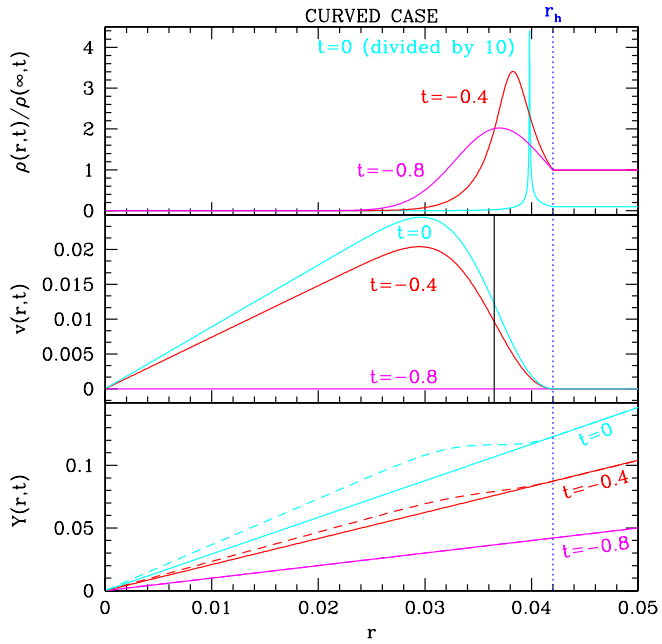

FIG. 6 (color online). Behavior of $Y(r, t)$ with respect to r, the peculiar velocities $v(r, t)$ with respect to r, and the density profiles $\rho(r, t)$ with respect to $r_{\mathrm{FRW}} = Y(r, t)/a(t)$, for the curved case at times $t = \bar{t} = -0.8$, $t = -0.4$, and $t = t_0 = 0$. The straight lines for $Y(r, t)$ are the FRW solutions while the dashed lines are the LTB solutions. For the peculiar velocities, the matter gradually starts to move toward high-density regions. The solid vertical line marks the position of the peak in the density with respect to r. For the densities, note that the curve for $\rho(r, 0)$ has been divided by 10. Finally, the values of $\rho(\infty, t)$ are 1, 2.8, and 25, for $t = 0$, -0.4, -0.8, respectively.

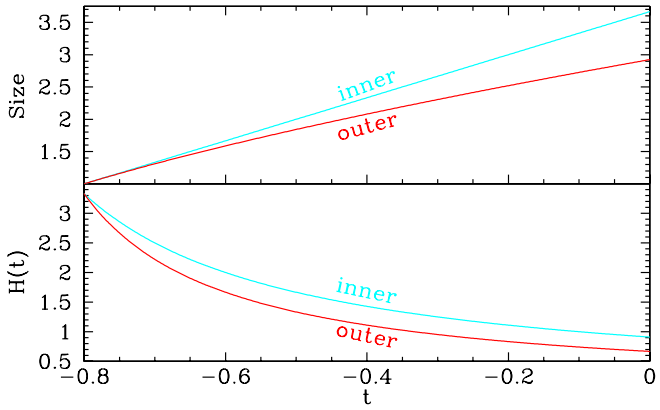

FIG. 7 (color online). Evolution of the expansion rate and the size for the inner and outer regions. Here "inner" refers to a point deep inside the hole, and "outer" refers to a point in the cheese.

case is useful to understand how the model behaves, and, in particular, the role of the curvature.

In Fig. 6 the results for $Y(r, t)$ in the curved case are plotted. Again time goes from $t = \bar{t} = -0.8$ to $t = 0$ (recall that $t_{BB} = -1$ and $t = 0$ is today).

As one can see, now the inner almost empty region is expanding faster than the outer (cheese) region. This is shown clearly in Fig. 7, where also the evolution of the inner and outer sizes is shown. Now the density ratio between the cheese and the interior region of the hole increases by a factor of 2 between $t = \bar{t}$ and $t = 0$. Initially the density ratio was 10^4, but the model is not sensitive to this number since the evolution in the interior region is dominated by the curvature ($k(r)$ is much larger than the matter density).

The peculiar velocities are now natural: as can be seen from Fig. 6, matter is falling towards the peak in the density. The evolution is now realistic, as one can see from Fig. 6, which shows the density profile at different times. Overdense regions start contracting and they become thin shells (mimicking structures), while underdense regions become larger (mimicking voids), and eventually they occupy most of the volume.

Let us explain why the high-density shell forms and the nature of the shell crossing. Because of the distribution of matter, the inner part of the hole is expanding faster than the cheese; between these two regions there is the initial overdensity. It is because of this that there is less matter in the interior part. (Remember that we matched the FRW density at the end of the hole.) Now we clearly see what is happening: the overdense region is squeezed by the interior and exterior regions which act as a clamp. Shell crossing eventually happens when more shells—each labeled by its own r—are so squeezed that they occupy the same physical position Y, that is when $Y' = 0$. Nothing happens to the photons other than passing through more shells at the same time: this is the meaning of the g_{rr} metric coefficient going to zero.

A remark is in order here: In the inner part of the hole there is almost no matter, it is empty. Therefore it has only negative curvature, which is largely dominant over the matter: it is close to a Milne universe.

IV. PHOTONS

We are mostly interested in observables associated with the propagation of photons in our Swiss-cheese model: indeed, our aim is to calculate the luminosity-distance-redshift relation $d_L(z)$ in order to understand the effects of inhomogeneities on observables. Our setup is illustrated in Fig. 8, where there is a sketch of the model with only 3 holes for the sake of clarity. Notice that photons are propagating through the centers.

We will discuss two categories of cases: (1) when the observer is just outside the last hole as in Fig. 8, and (2) when the observer is inside the hole. The observer in the hole will have two subcases: (a) the observer located on a high-density shell, and (b) the observer in the center of the hole. We are mostly interested in the first case: the observer is still a usual FRW observer, but looking through the holes in the Swiss cheese.

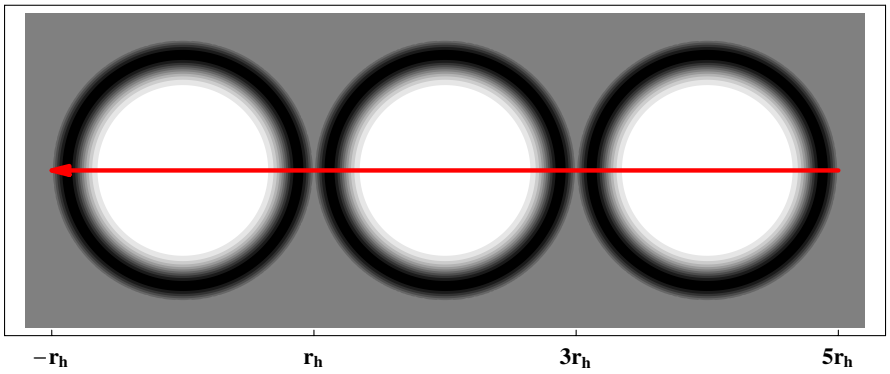

FIG. 8 (color online). Sketch of our model in comoving coordinates. The shading mimics the initial-density profile: darker shading implies larger denser. The uniform gray is the FRW cheese. The photons pass through the holes as shown by the arrow.

A. Finding the photon path: an observer in the cheese

We will discuss now the equations we will use to find the path of a photon through the Swiss cheese. The geodesic equations can be reduced to a set of four first-order differential equations (we are in the plane $\theta = \pi/2$):

$$\begin{aligned}
\frac{dz}{d\lambda} &= -\frac{\dot{Y}'}{Y'}\left((z+1)^2 - \frac{c_\phi^2}{Y^2}\right) - c_\phi^2\frac{\dot{Y}}{Y^3} && z(0) = 0,\\
\frac{dt}{d\lambda} &= z+1 && t(0) = t_0 = 0,\\
\frac{dr}{d\lambda} &= \frac{W}{Y'}\sqrt{(z+1)^2 - \frac{c_\phi^2}{Y^2}} && r(0) = r_h,\\
\frac{d\phi}{d\lambda} &= \frac{c_\phi}{Y^2} && \phi(0) = \pi,
\end{aligned} \tag{11}$$

where λ is an affine parameter that grows with time. The third equation is actually the null condition for the geodesic. Thanks to the initial conditions chosen we have $z(0) = 0$. These equations describe the general path of a photon. To solve the equations we need to specify the constant c_ϕ, a sort of angular momentum density. A first observation is that setting $c_\phi = 0$ allows us to recover the equations that describe a photon passing radially through the centers: $dt/dr = Y'/W$.

We are interested in photons that hit the observer at an angle α and are passing through all the holes as shown in Fig. 8. To do this we must compute the inner product of x^i and y^i, which are the normalized spatial vectors tangent to the radial axis and the geodesic as shown in Fig. 9. A similar approach was used in Ref. [7].

The inner product of x^i and y^i is expressed through

$$x^i = -\frac{W}{Y'}(1,0,0)|_{\lambda=0}, \tag{12}$$

$$y^i = \frac{1}{dt/d\lambda}\left(\frac{d}{d\lambda}, 0, \frac{d\phi}{d\lambda}\right)\Big|_{\lambda=0} = \left(\frac{dr}{d\lambda}, 0, \frac{d\phi}{d\lambda}\right)\Big|_{\lambda=0}, \tag{13}$$

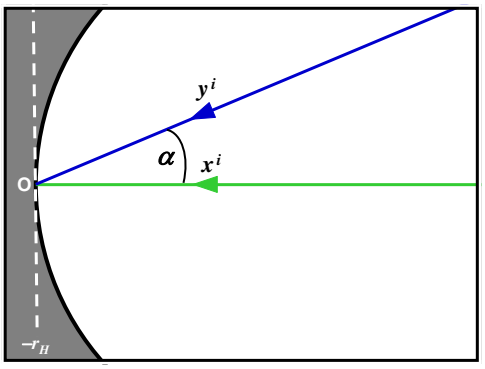

FIG. 9 (color online). A photon hitting the observer at an angle α.

$$x^i y^i g_{ij} = \frac{Y'}{W}\frac{dr}{d\lambda}\Big|_{\lambda=0} = \cos\alpha, \tag{14}$$

$$c_\phi = Y\sin\alpha|_{\lambda=0}. \tag{15}$$

The vectors are anchored to the shell labeled by the value of the affine parameter $\lambda = 0$, that is, to the border of the hole. Therefore, they are relative to the comoving observer located there. In the second equation we have used the initial conditions given in the previous set of equations, while to find the last equation we have used the null condition evaluated at $\lambda = 0$.

The above calculations use coordinates relative to the center. However, the angle α is a scalar in the hypersurface we have chosen: we are using the synchronous and comoving gauge. Therefore, α is the same angle measured by a comoving observer of Fig. 9 located on the shell $r = -r_h$: it is a coordinate transformation within the same hypersurface.

Given an angle α we can solve the equations. We have to change the sign in Eq. (11) when the photon is approaching the center with respect to the previous case where it is moving away. Also, we have to sew together the solutions between one hole and another, giving not only the right initial conditions, but also the appropriate constants c_ϕ (see Appendix B).

Eventually we end up with the solution $t(\lambda)$, $r(\lambda)$, $\phi(\lambda)$, and $z(\lambda)$ from which we can calculate the observables of interest.

B. Finding the photon path: an observer in the hole

Finding the solution in this case is the same as in the previous case with the only difference that in Eq. (11) the initial condition is now $r(0) = r_{\rm obs}$. But this observer has a peculiar velocity with respect to a FRW observer passing by. This, for example, will make the observer see an anisotropic cosmic microwave background as it is clear from Fig. 3. This Doppler effect, however, is already corrected in the solution we are going to find since we have chosen $z(0) = 0$ as initial condition.

There is, however, also the effect of light aberration which changes the angle α seen by the comoving observer with respect to the angle $\alpha_{\rm FRW}$ seen by a FRW observer. The photon can be thought as coming from a source very close to the comoving observer: therefore there is no peculiar motion between them. The FRW observer is instead moving with respect to this reference frame as pictured in Fig. 10. The relation between α and $\alpha_{\rm FRW}$ is given by the relativistic aberration formula:

$$\cos\alpha_{\rm FRW} = \frac{\cos\alpha + v/c}{1 + v/c\cos\alpha}. \tag{16}$$

The angle changes because the hypersurface has been changed. The velocity will be taken from the calculation (see Fig. 6 for the magnitude of the effect).

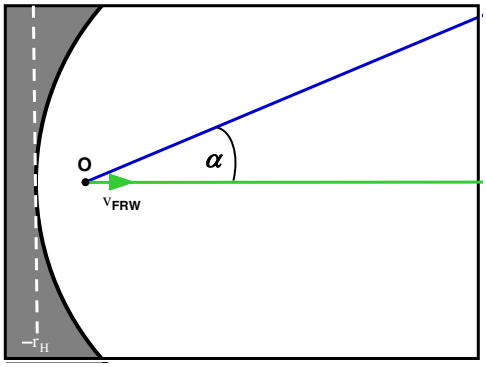

FIG. 10 (color online). A comoving observer and a FRW observer live in different frames, this results in a relative velocity v_{FRW} between observers.

C. Distances

The angular-diameter distance is defined as

$$d_A = \frac{D}{\alpha_{\mathrm{FRW}}}, \tag{17}$$

where D is the proper diameter of the source and α is the angle at which the source is seen by the observer. Using this definition to find d_A we have

$$d_A = \frac{2Y(r(\lambda), t(\lambda))\sin\phi(\lambda)}{2\alpha_{\mathrm{FRW}}}. \tag{18}$$

The luminosity distance will then be

$$d_L = (1+z)^2 d_A. \tag{19}$$

The formula we are going to use for d_A is exact in the limit of zero curvature. However in our model $E(r)$ is on average less than 0.3% and never more than 0.4%, as it can be seen from Fig. 4: therefore the approximation is good. Moreover, we are interested mainly in the case when the source is out of the last hole as pictured in Fig. 8, and in this case the curvature is exactly zero and the result is exact.

We have checked that the computation of d_A is independent of α for small angles and that the result using the usual FRW equation coincides with theoretical prediction for d_A. We also checked that d_A reduces to $Y(r, t)$ when the observer is in the center.

Finally we checked our procedure in comparison with the formula (E.31) of Ref. [8]: this is a rather different way to find the angular distance and therefore this agreement serves as a consistency check. We placed the observer in the same way and we found the same results provided that we use the angle α uncorrected for the light-aberration effect.

V. RESULTS: OBSERVER IN THE CHEESE

Now we will look through the Swiss cheese comparing the results with respect to a FRW-EdS universe and a ΛCDM case.

We will first analyze in detail the model with five holes, which is the one which we are most interested in. For comparison, we will study models with one big hole and one small hole. In the model with one big hole, the hole will be five times bigger in size than in the model with five holes: i.e., they will cover the same piece of the universe.

The observables on which we will focus are the changes in redshift $z(\lambda)$, angular-diameter distance $d_A(z)$, luminosity distance $d_L(z)$, and the corresponding distance modulus $\Delta m(z)$.

A. Redshift histories

Now we will first compare the redshift undergone by photons that travel through the model with either five holes or one hole to the FRW solution of the cheese. In Fig. 11 the results are shown for a photon passing through the center with respect to the coordinate radius. As one can see, the effects of the inhomogeneities on the redshift are smaller in the five-hole case.

It is natural to expect a compensation, due to the spherical symmetry, between the ingoing path and the outgoing one inside the same hole. This compensation is evident in Fig. 11.

However, there is a compensation already on the scale of half a hole as it is clear from the plots. This mechanism is due to the density profile chosen, that is one whose average matches the FRW density of the cheese: roughly speaking we know that $z' = H \propto \rho = \rho_{\mathrm{FRW}} + \delta\rho$. We chose the

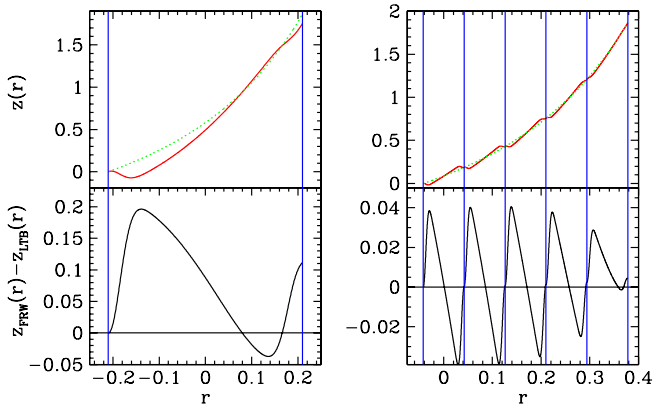

FIG. 11 (color online). Redshift histories for a photon that travels from one side of the one-hole chain (left) and five-hole chain (right) to the other where the observer will detect it at present time. The "regular" curve is for the FRW model. The vertical lines mark the edges of the holes. The plots are with respect to the coordinate radius r. Notice also that along the voids the redshift is increasing faster: indeed $z'(r) = H(z)$ and the voids are expanding faster.

density profile in order to have $\langle \delta\rho \rangle = 0$, and therefore in its journey from the center to the border of the hole the photon will see a $\langle H \rangle \sim H_{\rm FRW}$ and therefore there will be compensation for z'.

Let us see this analytically. We are interested in computing a line average of the expansion along the photon path in order to track what is going on. Therefore, we shall not use the complete expansion scalar:

$$\theta = \Gamma^k_{0k} = 2\frac{\dot{Y}}{Y} + \frac{\dot{Y}'}{Y'}, \tag{20}$$

but, instead, only the part of it pertinent to a radial line average:

$$\theta_r = \Gamma^1_{01} = \frac{\dot{Y}'}{Y'} \equiv H_r, \tag{21}$$

where Γ^k_{0k} are the Christoffel symbols and θ is the trace of the extrinsic curvature.

Using H_r, we obtain:

$$\langle H_r \rangle = \frac{\int_0^{r_h} dr H_r Y'/W}{\int_0^{r_h} dr Y'/W} \simeq \frac{\dot{Y}}{Y}\bigg|_{r=r_h} = H_{\rm FRW}, \tag{22}$$

where the approximation comes from neglecting the (small) curvature and the last equality holds thanks to the density profile chosen. This is exactly the result we wanted to find. However, we have performed an average at constant time and therefore we did not let the hole and its structures evolve while the photon is passing: this effect will partially break the compensation. This sheds light on the fact that photon physics seems to be affected by the evolution of the inhomogeneities more than by the inhomogeneities themselves. We can argue that there should be perfect compensation if the hole will have a static metric such as the Schwarzschild one. In the end, this is a limitation of our assumption of spherical symmetry.

This compensation is almost perfect in the five-hole case, while it is not in the one-hole case: in the latter case the evolution has more time to change the hole while the photon is passing. Summarizing, the compensation is working on the scale r_h of half a hole. These results are in agreement with Ref. [9].

From the plot of the redshift one can see that the function $z(r)$ is not monotonic. This happens at recent times when the high-density thin shell forms. This blueshift is due to the peculiar movement of the matter that is forming the shell. This feature is shown in Fig. 12 where the distance between the observer located just out of the hole at $r = r_h$ and two different shells is plotted. In the solid curve one can see the behavior with respect to a normal redshifted shell, while in the dashed curve one can see the behavior with respect to a shell that will be blueshifted: initially the distance increases following the Hubble flow, but when the shell starts forming, the peculiar motion prevails on the Hubble flow and the distance decreases during the collapse.

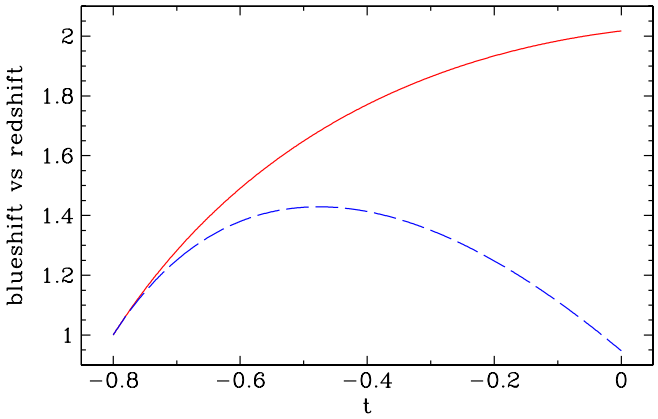

FIG. 12 (color online). Distance between the observer and two different shells. In the solid curve $r = 0.55 r_h$ will be redshifted, while in the dashed curve, $r = 0.8 r_h$ will be blueshifted. The latter indeed will start to collapse toward the observer. Time goes from $t = -0.8$ to $t = 0$. The observer is located just outside of the hole at $r = r_h$.

It is finally interesting to interpret the redshift that a photon undergoes passing the inner void. The small amount of matter is subdominant with respect to the curvature which is governing the evolution, but still it is important to define the space: in the limit of zero matter in the interior of the hole, we recover a Milne universe, which is just (half of) Minkowski space in unusual coordinates. Before this limit the redshift was conceptually due to the expansion of the spacetime, after this limit it is instead due to the peculiar motion of the shells which now carry no matter: it is a Doppler effect.

B. Luminosity and angular-diameter distances

1. The five-hole model

In Fig. 13 the results for the luminosity distance and angular distance are shown. The solution is compared to the one of the ΛCDM model with $\Omega_M = 0.6$ and $\Omega_{\rm DE} = 0.4$. Therefore, we have an effective $q_0 = \Omega_M/2 - \Omega_{\rm DE} = -0.1$. In all the plots we will compare this ΛCDM solution to our Swiss-cheese solution. The strange features which appear near the contact region of the holes at recent times are due to the nonmonotonic behavior of $z(r)$, which was explained in the previous section.

The distance modulus is plotted in the top panel of Fig. 13. The solution shows an oscillating behavior which is due to the simplification of this toy model in which all the voids are concentrated inside the holes and all the structures are in thin spherical shells. For this reason a fitting curve was plotted: it is passing through the points of the photon path that are in the cheese between the holes. Indeed, they are points of average behavior and represent well the coarse graining of this oscillating curve. The simplification of this model tells us also that the most interesting part of the plot is farthest from the observer,

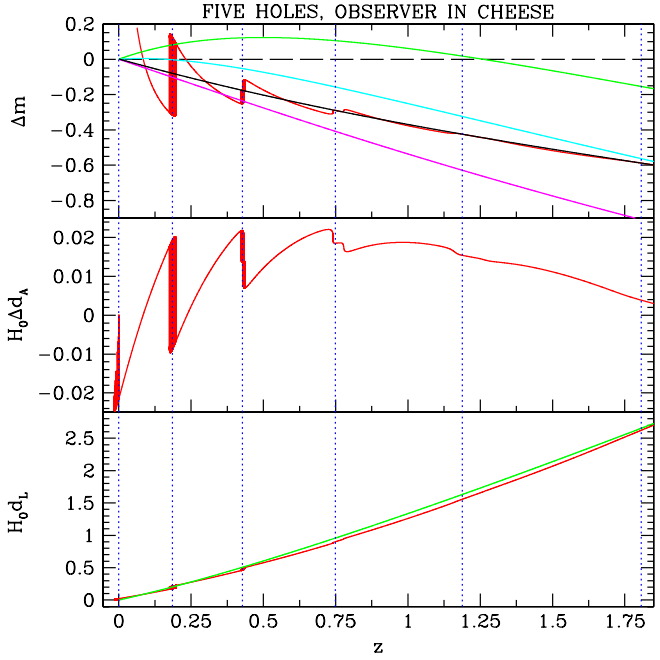

FIG. 13 (color online). On the bottom the luminosity distance $d_L(z)$ in the five-hole model (jagged curve) and the ΛCDM solution with $\Omega_M = 0.6$ and $\Omega_{\rm DE} = 0.4$ (regular curve) are shown. In the middle is the change in the angular-diameter distance, $\Delta d_A(z)$, compared to a ΛCDM model with $\Omega_M = 0.6$ and $\Omega_{\rm DE} = 0.4$. The top panel shows the distance modulus in various cosmological models. The jagged line is for the five-hole LTB model. The regular curves, from top to bottom, are a ΛCDM model with $\Omega_M = 0.3$ and $\Omega_{\rm DE} = 0.7$, a ΛCDM model with $\Omega_M = 0.6$ and $\Omega_{\rm DE} = 0.4$, the best smooth fit to the LTB model, and the EdS model. The vertical lines mark the edges of the five holes.

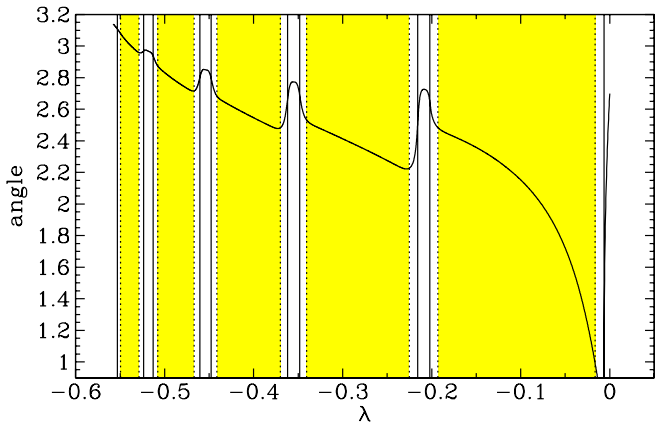

FIG. 14 (color online). The angle from the observer is plotted. The dashed vertical lines near the empty region mark the shell of maximum peculiar velocities of Fig. 6. The shaded regions represent the inner FRW solution. The solid vertical lines mark the peak in density. The angle at which the photon hits the observer is 2.7° on the left.

let us say at $z > 1$. In this region we can see the effect of the holes clearly: they move the curve from the EdS solution (in purple) to the ΛCDM one with $\Omega_M = 0.6$ and $\Omega_{\rm DE} = 0.4$ (in blue). Of course, the model is not realistic enough to reach the "concordance" solution.

Here we discuss a comparison of our results with those of Ref. [9]. In that paper they do not find the large difference from FRW results that we do. First of all, we note that we are able to reproduce their results using our techniques. The difference between their results and ours is that our model has very strong nonlinear evolution, in particular, close to shell crossing where we have to stop the calculation. The authors of Ref. [9] also used smaller holes with a different density/initial-velocity profile. This demonstrated that a large change in observables may require either nonspherical inhomogeneities, or evolution very close to shell crossing. (We remind the reader that caustics are certainly expected to form in cold dark matter models.)

Let us return now to the reason for our results. As we have seen previously, due to spherical symmetry there are no significant redshift effects in the five-hole case. Therefore, these effects must be due to changes in the angular-diameter distance. Figure 14 is useful to under-

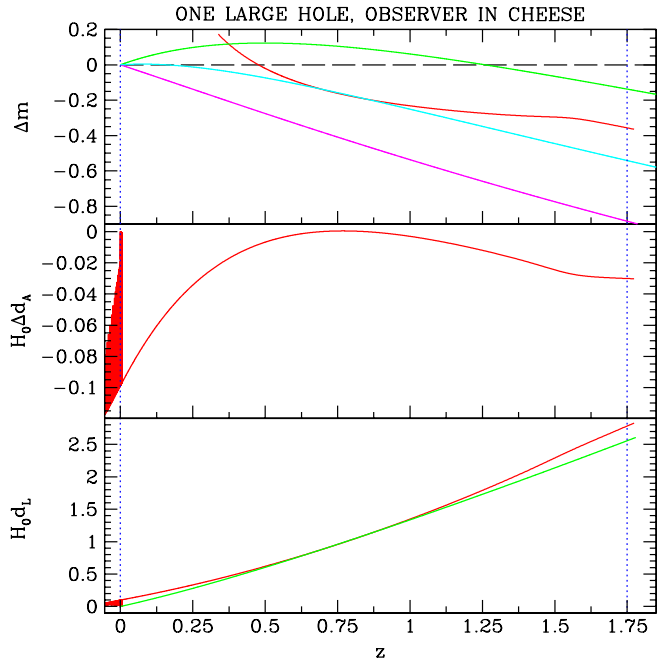

FIG. 15 (color online). On the bottom is shown the luminosity distance $d_L(z)$ in the one-hole model (jagged curve) and the ΛCDM solution with $\Omega_M = 0.6$ and $\Omega_{\rm DE} = 0.4$ (regular curve). In the middle is the change in the angular-diameter distance, $\Delta d_A(z)$, compared to a ΛCDM model with $\Omega_M = 0.6$ and $\Omega_{\rm DE} = 0.4$. On the top is shown the distance modulus in various cosmological models. The jagged line is for the one-hole LTB model. The regular curves, from top to bottom are a ΛCDM model with $\Omega_M = 0.3$ and $\Omega_{\rm DE} = 0.7$, a ΛCDM model with $\Omega_M = 0.6$ and $\Omega_{\rm DE} = 0.4$, and the EdS model. The vertical lines mark the edges of the hole.

stand what is going on: the angle from the observer is plotted. Through the inner void and the cheese the photon is going straight: they are both FRW solutions even if with different parameters. This is shown in the plot by constancy of the slope. The bending occurs near the peak in the density where the g_{rr} coefficient of the metric goes toward zero. Indeed the coordinate velocity of the photon can be split in an angular part: $v_\phi = d\phi/dt = 1/\sqrt{g_{\phi\phi}}$ and a radial part $v_r = dr/dt = 1/\sqrt{g_{rr}}$. While v_ϕ behaves well near the peak, v_r goes to infinity in the limit where shell crossing is reached: the photons are passing more and more matter shells in a short interval of time as the evolution approaches the shell-crossing point. Although in our model we do not reach shell crossing, this is the reason for the bending. We therefore see that all the effects in this model, redshift and angular effects, are due to the evolution of the inhomogeneities.

2. The one-hole model: The big hole case

Let us see now how the results change if instead of the five-hole model we use the one-hole model. We have already shown the redshift results in the previous section. As one can see from Fig. 15 the results are more dramatic: for high redshifts the Sswiss-cheese curve can be fit by a ΛCDM model with less dark energy than $\Omega_{\rm DE} = 0.6$ as in the five-hole model. Nonetheless, the results have not changed so much compared to the change in the redshift effects discussed in the previous section. Indeed the compensation scale for angular effects is $2r_h$ while the one for redshift effects is r_h.

3. The one-hole model: The small hole case

Finally if we remove four holes from the five-hole model, we lose almost all the effects. This is shown in Fig. 16: now the model can be compared to a ΛCDM model with $\Omega_M = 0.95$ and $\Omega_{\rm DE} = 0.05$.

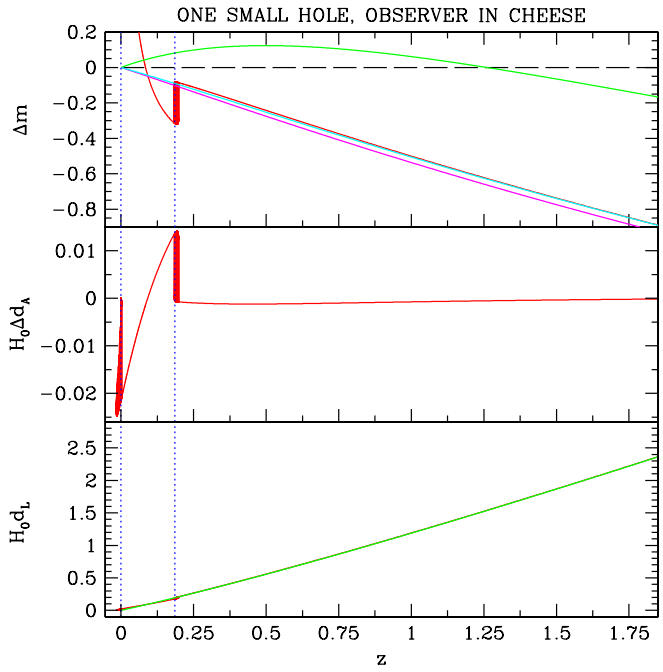

FIG. 16 (color online). On the bottom is shown the luminosity distance $d_L(z)$ in the one-hole model (jagged curve) and the ΛCDM solution with $\Omega_M = 0.95$ and $\Omega_{\rm DE} = 0.05$ (regular curve). In the middle is the change in the angular-diameter distance, $\Delta d_A(z)$, compared to a ΛCDM model with $\Omega_M = 0.95$ and $\Omega_{\rm DE} = 0.05$. On the top is shown the distance modulus in various cosmological models. The jagged line is for the one-hole LTB model. The regular curves, from top to bottom are a ΛCDM model with $\Omega_M = 0.3$ and $\Omega_{\rm DE} = 0.7$, a ΛCDM model with $\Omega_M = 0.95$ and $\Omega_{\rm DE} = 0.05$, and the EdS model. The vertical lines mark the edges of the hole.

VI. RESULTS: OBSERVER IN THE HOLE

Now we will examine the case in which the observer is inside the last hole in the five-hole model. We will first put the observer on the high-density shell and then place the observer in the center.

A. Observer on the high-density shell

In the section we show the results for the observer on the high-density shell. As one can see from Fig. 17, now the compensation in the redshift effect is lost: the photon is not completing the entire last half of the last hole. The results for the luminosity distance and the angular distance do not change much as shown in Fig. 18.

Remember that in this case the observer has a peculiar velocity compared to the FRW observer passing through the same point. We correct the results taking into account both the Doppler effect and the light-aberration effect.

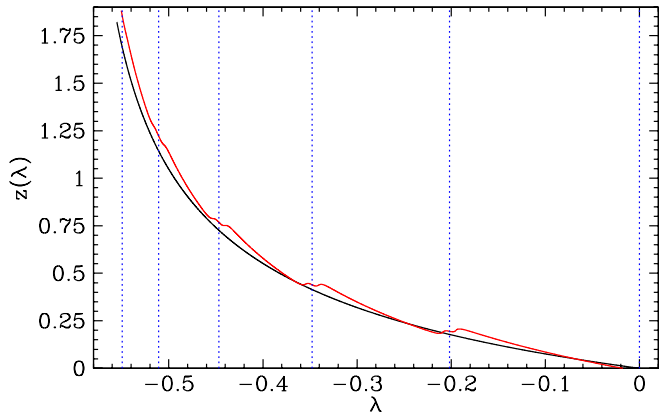

FIG. 17 (color online). Redshift histories for a photon that travels through the five-hole chain to the observer placed on the high-density shell. The regular line is for the FRW model. λ is the affine parameter and it grows with the time which goes from the left to the right. The vertical lines mark the end and the beginning of the holes.

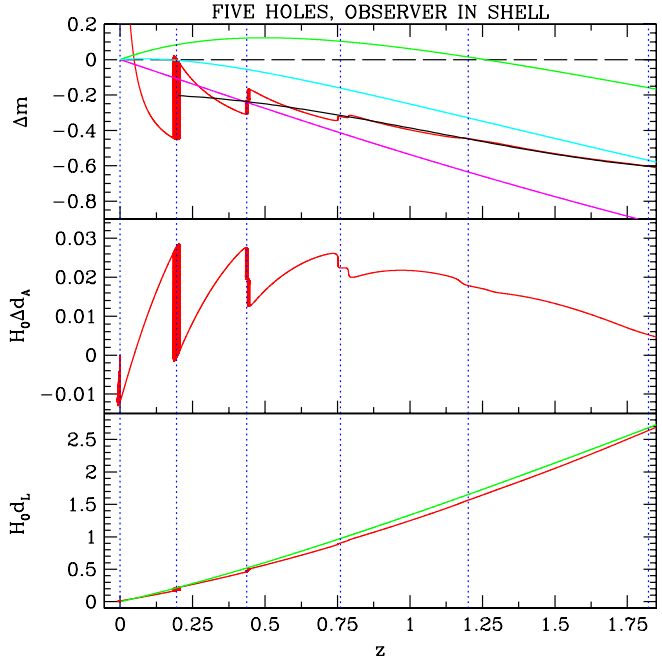

FIG. 18 (color online). On the bottom is shown the luminosity distance $d_L(z)$ in the five-hole model (jagged curve) and the ΛCDM solution with $\Omega_M = 0.6$ and $\Omega_{\rm DE} = 0.4$ (regular curve). In the middle is the change in the angular-diameter distance, $\Delta d_A(z)$, compared to a ΛCDM model with $\Omega_M = 0.6$ and $\Omega_{\rm DE} = 0.4$. On the top is shown the distance modulus in various cosmological models. The jagged line is for the five-hole LTB model. The regular curves, from top to bottom are a ΛCDM model with $\Omega_M = 0.3$ and $\Omega_{\rm DE} = 0.7$, a ΛCDM model with $\Omega_M = 0.6$ and $\Omega_{\rm DE} = 0.4$, the best smooth fit to the LTB model, and the EdS model. The vertical lines mark the edges of the five holes.

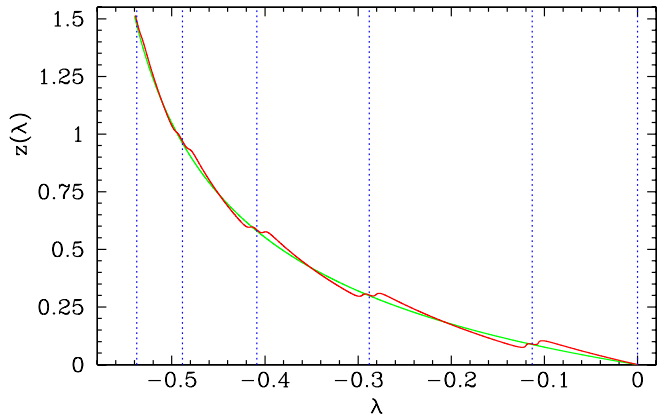

FIG. 19 (color online). Redshift histories for a photon that travels through the five-hole chain to the observer placed in the center. The regular line is for the FRW model. λ is the affine parameter and it grows with the time which goes from the left to the right. The vertical lines mark the end and the beginning of the holes.

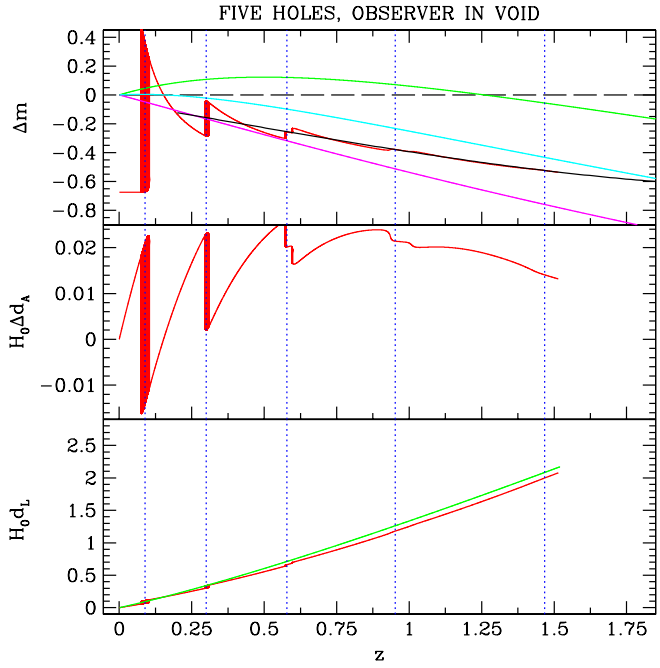

FIG. 20 (color online). The bottom panel shows the luminosity distance $d_L(z)$ in the five-hole model (jagged curve) and the ΛCDM solution with $\Omega_M = 0.6$ and $\Omega_{\rm DE} = 0.4$ (regular curve). In the middle is the change in the angular-diameter distance, $\Delta d_A(z)$, compared to a ΛCDM model with $\Omega_M = 0.6$ and $\Omega_{\rm DE} = 0.4$. On the top panel the distance modulus in various cosmological models is shown. The jagged line is for the five-hole LTB model. The regular curves, from top to bottom are a ΛCDM model with $\Omega_M = 0.3$ and $\Omega_{\rm DE} = 0.7$, a ΛCDM model with $\Omega_M = 0.6$ and $\Omega_{\rm DE} = 0.4$, the best smooth fit to the LTB model, and the EdS model. The vertical lines mark the edges of the five holes.

B. Observer in the center

In this section we show the results for the observer in the center. As confirmed by Fig. 19, the compensation in the redshift effect is good: the photon is passing through an integer number of half holes.

The results for the luminosity distance and the angular distance look worse as shown in Fig. 20, but this is mainly due to the fact that now the photon crosses half a hole less than in the previous cases and therefore it undergoes less bending.

In this case the observer has no peculiar velocity compared to the FRW one: this is a result of spherical symmetry.

VII. CONCLUSIONS

The aim of this paper was to understand the role of large-scale nonlinear cosmic inhomogeneities in the interpretation of observational data. This problem can be studied perturbatively; see, for example, Ref. [10]. Here, instead, we focused on an exact (even if toy) solution, based on the LTB model. This solution has been studied extensively in

the literature [7,8,11–18]. It has been shown that it can be used to fit the observed $d_L(z)$ without the need of dark energy (for example in [11]). To achieve this result, however, it is necessary to place the observer at the center of a rather big underdensity. To overcome this fine-tuning problem we built a Swiss-cheese model, placing the observer in the cheese and having the observer look through the Swiss-cheese holes as pictured in Fig. 8. A similar idea was at the basis of Refs. [9,19].

Summarizing, we first defined the model in Sec. II: it is a Swiss-cheese model where the cheese is made of the usual FRW solution and the holes are made of a LTB solution. We defined carefully the free functions of the LTB model in order to have a realistic (even if still toy) model and we showed its dynamics in Sec. III.

Then, as anticipated in the introduction, we focused on the effects of inhomogeneities on photons. The observables on which we focused are the change in redshift $\Delta z(\lambda)$ in angular-diameter distance $\Delta d_A(z)$, in the luminosity-distance-redshift relation $d_L(z)$, and in the distance modulus $\Delta m(z)$.

We found that redshift effects are suppressed when the hole is small because of a compensation effect acting on the scale of half a hole, due to spherical symmetry: it is roughly due to the fact that $z' = H \propto \rho = \rho_{\mathrm{FRW}} + \delta\rho$ and we chose the density profile in order to have $\langle \delta\rho \rangle = 0$. It is somewhat similar to the screening among positive and negative charges.

However, we found interesting effects in the calculation of the angular distance: the evolution of the inhomogeneities bends the photon path compared to the FRW case. Therefore, inhomogeneities will be able (at least partly) to mimic the effects of dark energy. We were mainly interested in making the observer look through the Swiss cheese from the cheese. However, for a better understanding, we examined also the case where the observer is inside the hole. We found bigger effects than those found in Refs. [9,19]: this could be due to the different model. Indeed, Refs. [9,19] used smaller holes with a different initial-density/initial-velocity profile.

ACKNOWLEDGMENTS

It is a pleasure to thank Alessio Notari and Marie-Noelle Célérier for useful discussions and suggestions. V. M. acknowledges support from "Fondazione Ing. Aldo Gini" and "Fondazione Angelo Della Riccia."

APPENDIX A: ABOUT THE ARBITRARY FUNCTIONS IN A LTB MODEL

Here we illustrate, by means of an example, the choice of the arbitrary functions in LTB models. We are going to analyze the flat case. Indeed we have an analytical solution for it and this will help in understanding the issues.

We said previously that there are three arbitrary functions in the LTB model: $\rho(r)$, $W(r)$, and $\bar{t}(r)$. They specify the position and velocities of the shells at a chosen time. In general, $\bar{t}$ depends on r; because of the absence of shell crossing it is possible to give the initial conditions at different times for different shells labeled by r.

We start, therefore, by choosing the curvature $E(r) = (W^2(r) - 1)/2$ to vanish, which can be thought as a choice of initial velocities $\dot{Y}$ at the time $\bar{t}(r)$:

$$2E(r) = \dot{Y}^2 - \frac{1}{3\pi}\frac{M}{Y}\bigg|_{r,\bar{t}(r)}. \tag{A1}$$

For $E(r) = 0$, the model becomes

$$ds^2 = -dt^2 + dY^2 + Y^2 d\Omega^2, \tag{A2}$$

with solution

$$\begin{aligned} Y(r,t) &= \left(\frac{3M(r)}{4\pi}\right)^{1/3}[t - \hat{t}(r)]^{2/3}, \\ \bar{\rho}(r,t) &= [t - \hat{t}(r)]^{-2}, \end{aligned} \tag{A3}$$

where

$$\begin{aligned} \hat{t}(r) &\equiv \bar{t}(r) - \bar{\rho}^{-1/2}(r, \bar{t}(r)), \\ \bar{\rho}(r, \bar{t}(r)) &= \frac{3M(r)}{4\pi}\frac{1}{Y^3}\bigg|_{r,\bar{t}(r)}. \end{aligned} \tag{A4}$$

The next step is to choose the position of the shells, that is, to choose the density profile. As far as $\bar{t}(r)$ is concerned, only the combination $\hat{t}(r)$ matters. This, however, is not true for $M(r)$, which appears also by itself in Eq. (A3).

Looking at Eq. (A4) we see that to achieve an inhomogeneous profile we can either assign a homogeneous profile at an inhomogeneous initial time, or an inhomogeneous density profile at a homogeneous initial time, or both. Moreover, if we assign the function $M(r)$, then we can use our freedom to relabel r in order to obtain all the possible $\bar{t}(r)$. So we see that one of the three arbitrary functions expresses the gauge freedom.

In this paper we fixed this freedom by choosing $\bar{t}(r) = \bar{t}$ and $Y(r, \bar{t}) = r$ in order to have a better intuitive understanding of the initial conditions.

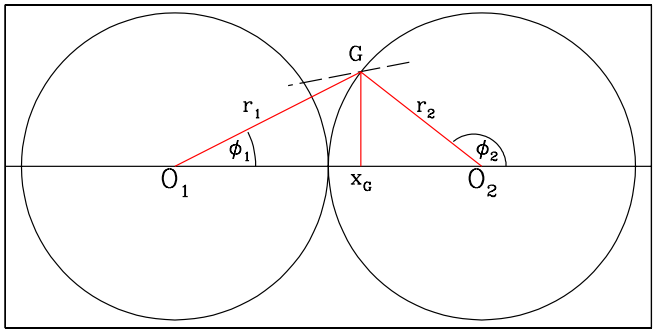

FIG. 21 (color online). Illustration of the procedure to calculate the transition between two holes. The dashed line is a segment of the geodesic. O_1 and O_2 represent the two coordinate systems.

APPENDIX B: SEWING THE PHOTON PATH

In the appendix we will demonstrate how to sew together the photon path between two holes. We will always use center-of-symmetry coordinates, and therefore we will move from the coordinates of O_1 to the ones of O_2 illustrated in Fig. 21. The geodesic near the contact point G is represented by the dashed line segment in Fig. 21.

First, we want to find the value $\bar{\lambda}$ of the affine parameter for which the photon is at G. This is found solving

$$\begin{aligned} &G_2 = (r_1(\lambda)\cos\phi_1(\lambda) - 2r_h, r_1(\lambda)\sin\phi_1(\lambda)), \\ &r_h^2 = x_{2G}^2 + y_{2G}^2. \end{aligned} \tag{B1}$$

These equations imply

$$r_1^2(\lambda) + 3r_h^2 - 4r_1(\lambda)r_h\cos\phi_1(\lambda) = 0. \tag{B2}$$

Then we can give the initial conditions for the second hole:

$$\begin{aligned} &q_2(\bar{\lambda}) = q_1(\bar{\lambda}), \qquad t_2(\bar{\lambda}) = t_1(\bar{\lambda}), \\ &r_2(\bar{\lambda}) = r_h, \qquad \phi_2(\bar{\lambda}) = \arccos(x_{2G}/r_h). \end{aligned} \tag{B3}$$

Finally, we need the constant c_ϕ, a sort of constant angular momentum density. Repeating the procedure of Sec. IV A for the first hole we find

$$c_{2\phi} = \sin\alpha_2 q_1(\bar{\lambda}) Y_2|_{\bar{\lambda}}. \tag{B4}$$

Only α_2 is missing. One way to find it is to calculate the inner product in O_1 coordinates of the geodesic with the normalized spatial vector parallel to $\overline{O_2G}$ (see Fig. 21).

[1] T. Buchert, arXiv:0707.2153.
[2] A. G. Lemaitre, Gen. Relativ. Gravit. **29**, 641 (1997); Ann. Soc. Sci. Bruxelles A **53**, 51 (1933).
[3] R. C. Tolman, Proc. Natl. Acad. Sci. U.S.A. **20**, 169 (1934).
[4] H. Bondi, Mon. Not. R. Astron. Soc. **107**, 410 (1947).
[5] A. Einstein and E. G. Straus, Rev. Mod. Phys. **17**, 120 (1945).
[6] To get this number from Table I you need to multiply r_h by $a(t_0) \simeq 2.92$.
[7] H. Alnes and M. Amarzguioui, Phys. Rev. D **74**, 103520 (2006).
[8] T. Biswas, R. Mansouri, and A. Notari, arXiv:astro-ph/0606703.
[9] T. Biswas and A. Notari, arXiv:astro-ph/0702555.
[10] E. W. Kolb, S. Matarrese, and A. Riotto, New J. Phys. **8**, 322 (2006).
[11] H. Alnes, M. Amarzguioui, and O. Grøn, Phys. Rev. D **73**, 083519 (2006).
[12] M. N. Célérier, Astron. Astrophys. **353**, 63 (2000).
[13] R. Mansouri, arXiv:astro-ph/0512605.
[14] R. A. Vanderveld, E. E. Flanagan, and I. Wasserman, Phys. Rev. D **74**, 023506 (2006).
[15] S. Rasanen, J. Cosmol. Astropart. Phys. 11 (2004) 010.
[16] K. Tomita, Prog. Theor. Phys. **106**, 929 (2001).
[17] D. J. H. Chung and A. E. Romano, Phys. Rev. D **74**, 103507 (2006).
[18] T. Kai, H. Kozaki, K. Nakao, Y. Nambu, and C. Yoo, Prog. Theor. Phys. **117**, 229 (2007).
[19] N. Brouzakis, N. Tetradis, and E. Tzavara, J. Cosmol. Astropart. Phys. 02 (2007) 013.